Electronic supplementary materials

For https://doi.org/10.1631/jzus.A2300183

A novel approach for the optimal arrangement of tube bundles in a 1000-MW condenser

Jinju GUO[1], Taoye YIN[1], Shuai WANG[1], Wei CHEN[1], Peiwang ZHU[1], Kun LUO[1,2]✉,Yun KUANG[3], Jie LIU[3], Junjun HUANG[3], Bing HUO[4], Hui WANG[3], Chunlin ZHANG[5], Jian WANG[3]

[1]*State Key Laboratory of Clean Energy Utilization, Zhejiang University, Hangzhou 310027, China*

[2]*Shanghai Institute for Advanced Study of Zhejiang University, Shanghai 200120, China*

[3]*Central Southern China Electric Power Design Institute Co., Ltd. of China Power Engineering Consulting Group, Wuhan 430071, China*

[4]*Huanggang Dabieshan Power Generation Co., Ltd, Huanggang 438300, China*

[5]*China Energy Digital Technology Group Co., Ltd, Beijing 100022, China*

S1 Mathematical model

The mathematical model is established with the following assumptions (Sadek et al., 2018):

(1) The condensation film is neglected, and the shell-side flow is assumed to be a mixture of water vapour and air;

(2) The air is assumed to be introduced from the inlet and evenly mixed with the turbine exhaust vapour at the same velocity.

(3) The steam is considered to condense only around the tubes. The condensation effect is considered by adding a source term in the mass and momentum conservation equations.

(4) The temperature of the mixture at each location on the shell side of the condenser corresponds to the saturation temperature of the partial pressure of water vapour at that location. In other words, the water vapour at each location is condensed in a saturated state.

(5)

S1.1 Governing equations of the fluid phase

According to assumption (4), the temperature of the fluid phase is determined by the corresponding partial pressure of the water vapour, thus, it is unnecessary to solve the energy conservation equation. Accordingly, the governing equations of the fluid phase including the mass conservation, momentum conservation, and species conservation equations are given by:

$$\frac{\partial \rho}{\partial t}+\nabla\cdot\left(\rho\mathbf{U}\right)=S_m \tag{S1}$$

$$\frac{\partial\left(\rho\mathbf{U}\right)}{\partial t}+\nabla\cdot\left(\rho\mathbf{U}\mathbf{U}\right)=\nabla\cdot\tau+\mathbf{F}-\nabla p \tag{S2}$$

$$\frac{\partial(\rho Y_i)}{\partial t} + \nabla \cdot (\rho \mathbf{U} Y_i) = \nabla \cdot (D_i \nabla Y_i) + S_i \quad \text{(S3)}$$

where ρ, **U**, and p are the density, velocity vector, and pressure of the fluid phase, respectively. τ is the stress tensor of the fluid phase, correlating with the molecular viscosity (μ_f) and turbulent viscosity ($\mu_t = c_\mu \rho k^2/\varepsilon$), in which the turbulence kinetic energy (k) and turbulence dissipation rate (ε) are calculated by a realizable k-ε turbulence model (Sokolichin and Eigenberger, 1999). S_m, **F**, and S_i are the source items of the mass, momentum, and species, respectively. Specifically, S_m represents the volumetric condensation rate of water vapour, given by:

$$S_m = \rho U A_{area} / V_{cell} \quad \text{(S4)}$$

where V_{cell} is the volume of a specific cell adhering to the wall. A_{area} is the projection area of this cell to the wall. Y_i and D_i are the mass fraction and mass diffusion coefficient of species i, respectively. The investigated object is the condenser, in which the fluid phase is a mixture of water vapour and air. The air concentration is tiny as compared with the water vapour, thus, the species conversation equation corresponds to the transport equation of the air.

S1.2 Phase change model

In this work, the outline of the tube bundle arrangement along the periphery of all tube bundles is drawn, which is used to divide the flow field on the shell side of the condenser into two types of regions. The first region is the condensation region in the tube bundle zone, which refers to the shell side region including the cooling tube inside the outline, where water vapour condensation occurs, and fine grids are used. The second region is the non-condensing region of the steam channel, which refers to the zone outside the outline and does not contain cooling tubes. There is no phase change in this region, and the coarse grids are used to reduce computational costs. Assuming that there is no slip between the gas-liquid two phases, the total pressure at the gas-liquid interface is equal to the mainstream area of the gas mixture, and the latent heat released by the condensation of the water vapour is all transferred through the conduction of the liquid film, and the surface temperature of the liquid film is the saturation temperature of the water vapour at the corresponding partial pressure. After the condensate is generated, it will be discharged from the flow field.

In the condensation zone of the tube bundle, the mass flow rate of water vapour condensed in unit control volume can be added as a source term to the mass conservation equation of water vapour in the gas mixture. According to Newton's law of cooling, the amount of heat released during the condensation is $Q = \dot{m}L$. $\dot{m}$ represents the condensation rate, which is a negative value due to the reduction of the water vapour. The heat transfer through the wall of a condenser at a given location is $Q = h\Delta t_m A$. According to the law of energy conservation, $Q = \dot{m}L = h\Delta t_m A$. The mass flow rate of condensation in the condensing area is expressed as:

$$\dot{m} = \frac{\Delta t_m A}{R_{total} L} \quad \text{(S5)}$$

where Δt_m is the temperature difference and A is the area of the heat transfer area.

Thermal resistance during the condensation process is considered by implementing empirical equations into the governing equations for calculating the condensation amount of water vapour. As shown in Fig. S1, the total thermal resistance R_{total} ($=R_{cw}+R_w+R_c+R_a$) includes the resistance of cooling water R_{cw}, the resistance of the tube wall R_w, the resistance of the condensation film R_c, and the resistance of non-condensable air R_a. The detailed calculations for these items are given below.

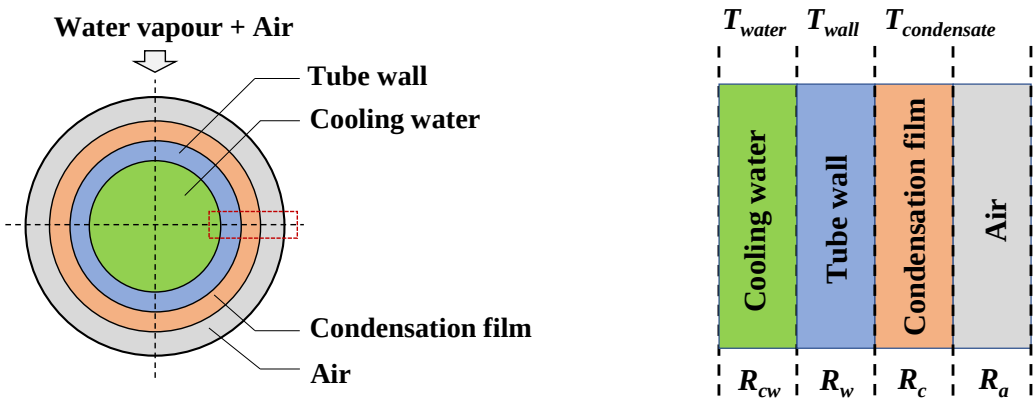

Fig. S1 Thermal resistances during condensation outside the tube: (a) cross-section of a tube; (b) 1D view

The convection-induced thermal resistance of the cooling water R_{cw} is calculated as (Gnielinski, 1975):

$$\frac{1}{R_{cw}}=\frac{d_{in}}{d_{out}}\left[\frac{\lambda_{cw}}{8d_{in}}\frac{\varepsilon \mathrm{Re}_{cw}\mathrm{Pr}_{cw}}{K_1+K_2\left(\varepsilon/8\right)^{0.5}\left(\mathrm{Pr}_{cw}^{-2/3}-1\right)}\right] \tag{S6}$$

where ε = $(1.82\lg \mathrm{Re}_{cw}\text{-}1.64)^{-2}$, K_1 = 1+3.4ε, K_2=11.7+1.8$\mathrm{Pr}_{cw}^{-1/3}$. d_{in} and d_{out} are the inner and outer diameters of the tube, respectively. λ_{cw}, Re_{cw} and Pr_{cw} are the thermal conductivity, the Reynolds number, and the Prandtl number of tube-side cooling water, respectively.

The conduction-induced thermal resistance of the tube wall R_w is calculated as (Incropera et al., 1996):

$$\frac{1}{R_w}=\frac{2\lambda_w}{d_{out}\ln\left(d_{in}/d_{out}\right)} \tag{S7}$$

where λ_w is the thermal conductivity of the tube wall.

The thermal resistance of the condensed liquid film attached to the outer surface of the tube R_c is calculated by (Mirzabeygi and Zhang, 2015):

$$\frac{1}{R_c}=\frac{1}{R_{co}}\left(1+0.0095\mathrm{Re}^{11.8/\sqrt{\mathrm{Nu}}}\right)N^{-0.16} \tag{S8}$$

where R_{co} is the thermal resistance of condensation film considering the laminar steam outside the horizontal tube. $\left(1+0.0095\mathrm{Re}^{11.8/\sqrt{\mathrm{Nu}}}\right)$ is the correction of the shear effect of the steam to the liquid film, where Nu = $(d_{out}/R_{co}\lambda)$ is the Nusselt number of the laminar liquid film. $N^{-0.16}$ is the correction coefficient for the tube bundle effect, where N is the number of tube rows counted from the top to the bottom. R_{co} is calculated by (Popiel and Boguslawski, 1975):

$$\frac{1}{R_{co}}=0.725\left[\frac{g\lambda_c^{\,3}\rho_c^{\,2}L}{d_o\mu_c(T_{cs}-T_w)}\right]^{1/4} \tag{S9}$$

where g is the gravitational acceleration. λ_c, ρ_c and μ_c are the thermal conductivity, density, and molecular viscosity of the condensing film, respectively. L is the latent heat of phase change. T_{cs} and T_w are the surface temperature of the condensation film and tube wall, respectively.

The convection-induced thermal resistance of the air film with a high air concentration on the outer surface of the tube R_a is calculated as (Ghiaasiaan, 2007):

$$\frac{1}{R_a}=a\frac{D_k}{d_{out}}Re^{0.5}\left(\frac{P_{mixture}}{P_{mixture}-P_{vapor}}\right)^b P_{mixture}^{\frac{1}{3}}\left(\frac{\rho_s L}{T_s}\right)^{\frac{2}{3}}\left(T_s-T_{cs}\right)^{-\frac{1}{3}} \tag{S10}$$

where D_k is the mass diffusion coefficient. P_{vapor} is the steam fractional pressure in the mixture. T_s is the saturation temperature of the steam. a and b are empirical constants, where a = 0.82 and b = 0.6.

When water vapour encounters a wall below its dew point temperature, condensation occurs and the latent heat is released. The temperature gradient within the liquid film transfers heat from the interface to the wall. The liquid film is the main thermal resistance of condensation heat transfer of the pure water vapour. Non-condensable air severely impairs condensation heat transfer. The gas mixture reaches the surface of the liquid film through convective mass transfer, and the water vapour undergoes a condensation process, while the non-condensable air cannot penetrate the liquid film and continuously accumulates on the interface. The only way for non-condensable air to leave the interface is to diffuse into the main flow region, for which a sufficiently large concentration gradient is required. Since the air diffusion equation is being solved, there is no component source term in the tube bundle region.

S1.3 Numerical procedure

As the computational costs are unaffordable for simulating such a full 3D condenser, a simplified 2D apparatus is established by implementing the phase change model via a UDF on the commercial software package ANSYS Fluent. A realizable k-ε turbulence model is adopted for calculating fluid turbulence. The convection term is discretised by a first-order upwind scheme while the diffusion term is discretised by a second-order central differencing scheme. A SIMPLE algorithm is used to handle the pressure-velocity coupling. The specific heat capacities of the species and mixture are evaluated by a piecewise polynomial fitting method and a mixing law, respectively. The density of the gas mixture is calculated using an ideal gas law. The thermal conductivity and viscosity are calculated as a mass-fraction-weighted average of all species. The mass diffusivity of the gas mixture is calculated by kinetic theory. The residuals of all governing equations are specified to be less than 10^{-6} to ensure numerical convergence.

S2 Computational settings

S2.1 Simulation conditions

The investigated object is a 1000 MW double back pressure condenser, which is designed by Shanghai Electric Power Generation Equipment Co., Ltd. Fig. S2(a) presents a 3D view of the condenser situated amidst a set of tube bundles arranged in parallel with a length of 13.3 m. To minimize computational expenses, a 2D simulation of this condenser is conducted. This decision is based on two factors: (i) the high computational expenses of a complete 3D simulation, which is prohibitively expensive for most academic and engineering researchers, and (ii) the minor impact on thermophysical properties owing to the condenser's considerable depth (i.e., 13.3 m). The flow dynamics and heat transfer around each tube are minimally influenced by the rear and back walls. Fig. S2(b) shows the configuration of the 2D condenser. Considering the symmetry of the tube bundle, the computational domain is one-sixteenth of the tube bundle of the condenser (except the throat). The air leakage parameter holds significant importance, as it directly influences the heat transfer coefficient. Although pure steam can be condensed without any non-condensing air, a small amount of air inevitably leaks into the shell-side flow field due to practical operating conditions, which reduces the heat transfer efficiency of the condenser. To address this issue, it is necessary to improve the tightness of the condenser. However, it is important to achieve a balance between tightness and heat transfer efficiency. In this study, the rated air leakage (i.e., γ_{air}) of the investigated 1000 MW condenser is specified as 8×10^{-5}, representing the most acceptable air leakage volume. Under the condition of rated air leakage ($\gamma_{air} = 8 \times 10^{-5}$), the gas mixture of air and water vapour flows through the main tube bundle area and passes through the internal baffle and air-cooling area to reach the exit. The tubes in the investigated condenser are arranged in a uniform manner and a non-uniform manner, as shown in Fig. S2(c, d). For the uniform tube bundle arrangement, the adjacent tubes are arranged in an equilateral

triangle with a pitch of 32mm. For the non-uniform tube bundle arrangement, the adjacent tubes are arranged in an isosceles triangle with pitches of 32 mm and 39 mm. More detailed information on the tube bundle arrangement can refer to Fig. S3 and Fig. S4. The boundary conditions and physical parameters required for the numerical simulation were set based on relevant data obtained from the practical operation of the condenser, as listed in Table S1. Combining the inlet mass flow rate and the physical parameters of the water vapour, the inlet velocity is calculated as 52 m/s. The outlet pressure of the condenser is taken as 4410 Pa (absolute pressure). Detailed operating parameters are listed in Table S2.

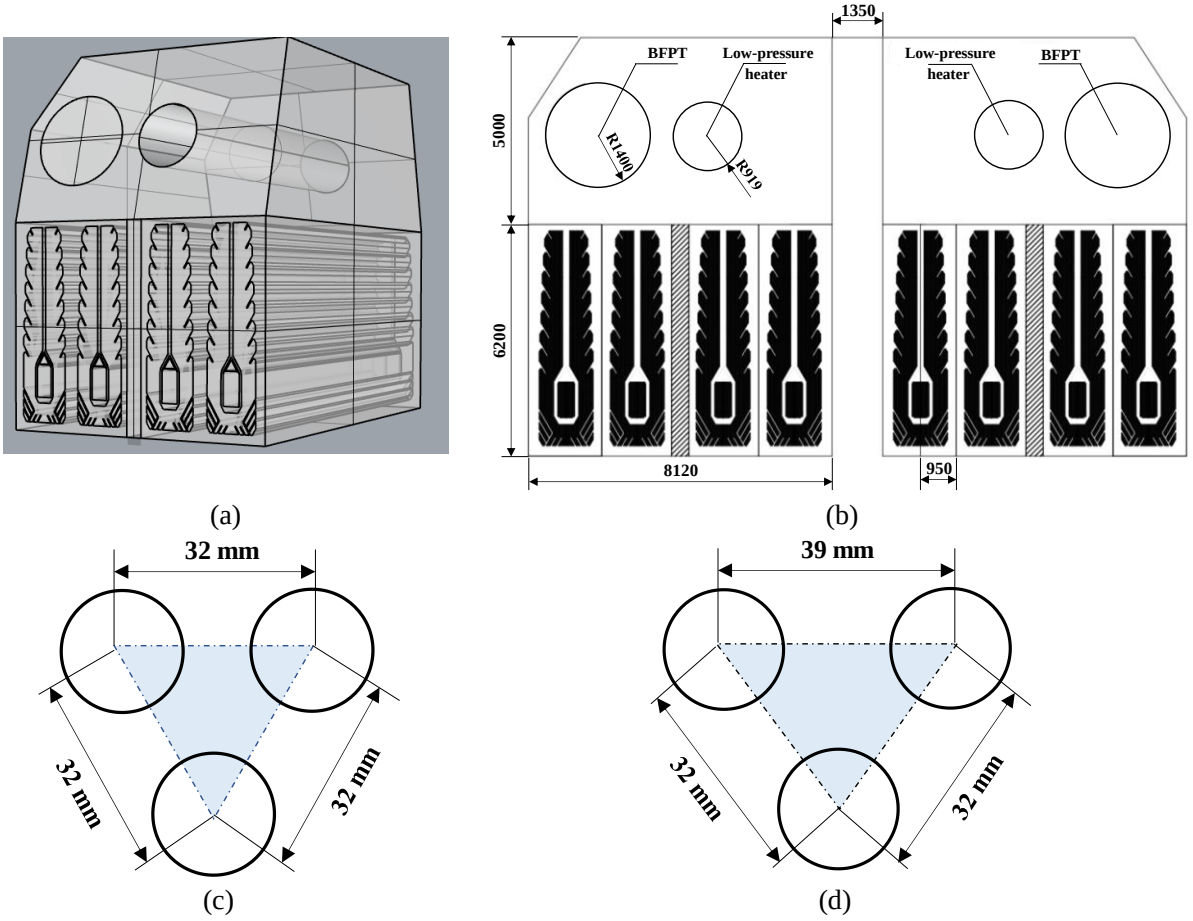

Fig. S2 (a) 3D view of the investigated 1000 MW condenser; (b) The investigated 1000MW condenser (BFPT: boiler feed-water pump turbine); (c) schematic of the uniform tube bundle arrangement; (d) schematic of the non-uniform tube bundle arrangement

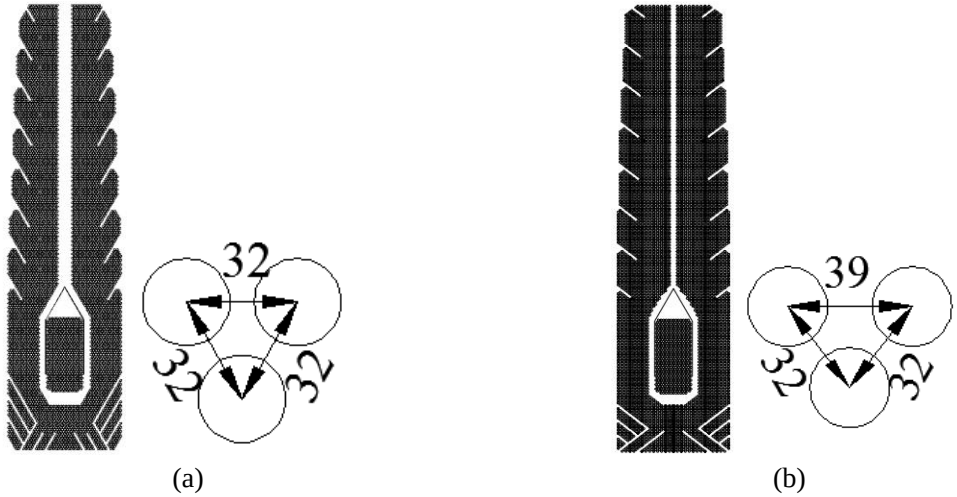

Fig. S3 Computational grids of the condenser: (a) uniform tube bundle arrangement; (b) non-uniform tube bundle arrangement

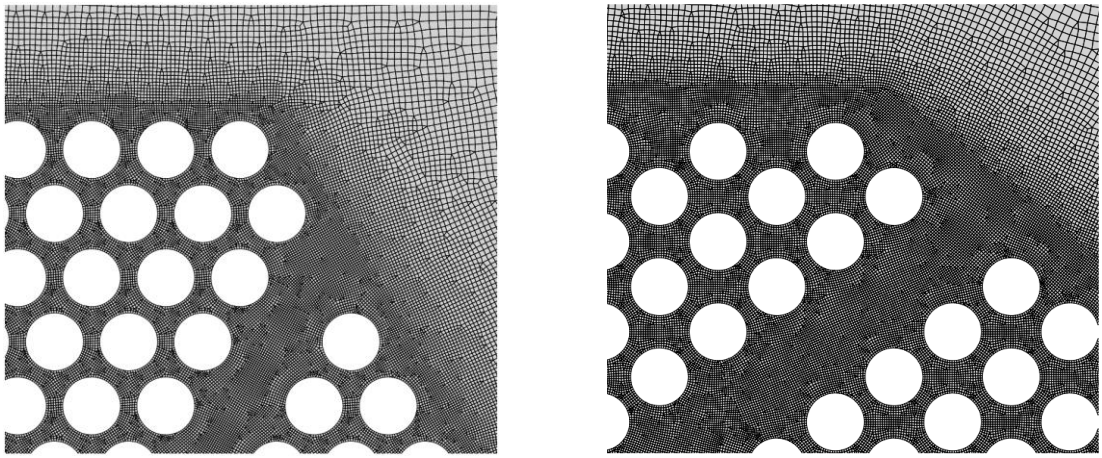

(a) (b)

Fig. S4 Computational grids of the local zone of the condenser: (a) uniform tube bundle arrangement; (b) non-uniform tube bundle arrangement

Table S1 Designed operating parameters of the condenser

Parameter	Value	Unit
Average back pressure of main engine low-pressure cylinder exhaust	5.26	kPa
Enthalpy of main engine low-pressure cylinder exhaust	2330.6	kJ/kg
Flow rate of main engine low-pressure cylinder exhaust	413.067	kg/s
Dryness of main engine low-pressure cylinder exhaust	90	%
Pressure of water pump steam turbine exhaust	6.26	kPa
Flow rate of water pump steam turbine exhaust	20.893	kg/s
Dryness of main engine low-pressure cylinder exhaust	95.36	%

Table S2 Operating parameters in the simulation

Parameter	Value	Unit
Inlet temperature	307.45	K
Inlet velocity	52	m/s
Inlet air mass fraction	8×10^{-5}	-
Tube temperature	300.689	K
Outlet absolute pressure	4410	Pa

The boundary conditions should be properly set before the simulation. For the velocity, the inlet is specified with a uniform velocity boundary condition, and the outlet is assigned with a zero-gradient velocity boundary condition. For the pressure, the inlet is specified as a zero-gradient pressure boundary condition and the outlet is set as a fixed pressure boundary condition. The wall is specific as a non-slip boundary condition.

S2.2 Gird-independence analysis

The grid-dependence analysis is conducted before the simulation. For the scenario where the air leakage is 0.00008, the half region of a tube bundle with a 2D configuration (i.e., 950 mm×6200 mm) is divided into unstructured grids, as shown in Fig. S5. To better discuss the heat transfer of each tube, the tube bundle is divided into 10 zones from top to bottom, among which Condenser10 is the air-cooling zone,

the air extraction port is located in the air-cooling zone, and the air-cooling zone is the last section where the water vapour flows out of the tube bundle. The quantity and quality of computational grids determine the accuracy of CFD simulations. In this work, the meshes around each tube are refined to better capture the condensation process on the surface of the tube bundles. The grid density near the surface has a mesh density 7 times higher than the rest of the region. Four groups of grid resolutions are assigned for the grid-independence analysis, as listed in Table S3.

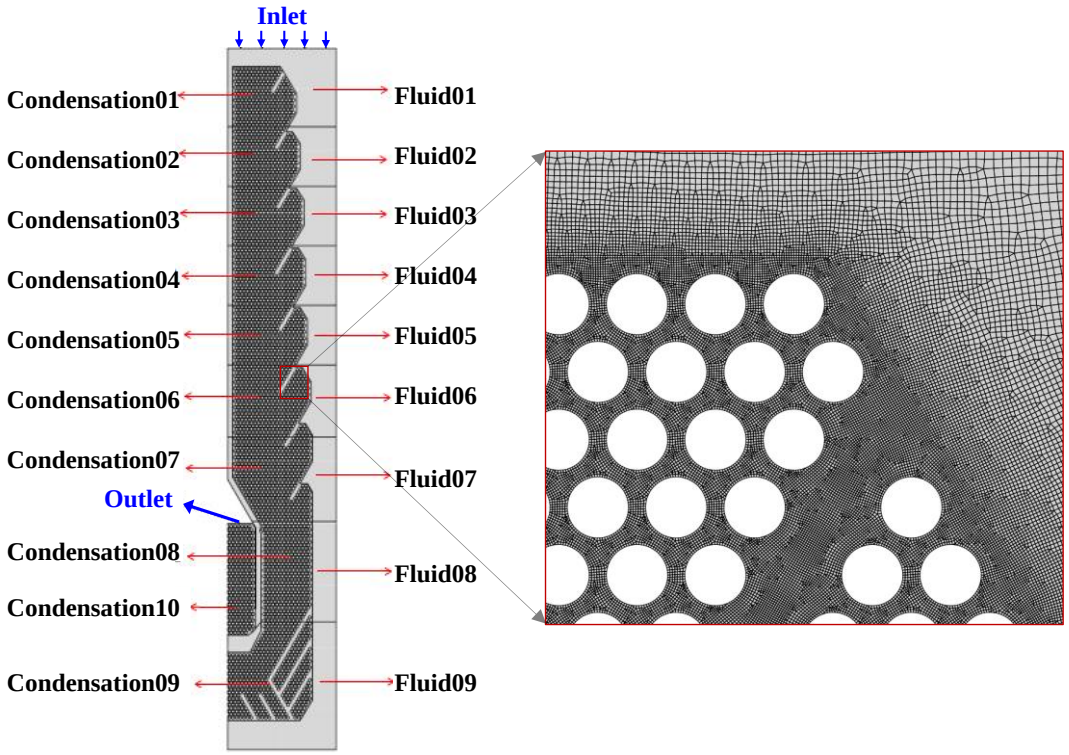

Fig. S5 Computational grids of the tube bundle, where the computational domain is marked with Condensation01~09 and Fluid01~09 according to the different zones

Table S3 Grid properties for grid-independence analysis

Label	Size of cells in condensation zones	Size of cells in non-condensation zones	Number of cells
Mesh1	2 mm	8 mm	693 646
Mesh2	1 mm	16 mm	2 168 722
Mesh3	1 mm	8 mm	2 298 829
Mesh4	1 mm	4 mm	2 586 023

Fig. S6 shows the pressure drop and heat transfer coefficient under different grid resolutions. It is noted that the numerical results from the coarse grid (i.e., Mesh1) show the largest discrepancy with that from other grids (i.e., Mesh2~Mesh4). Refining grids from Mesh2 to Mesh4 shows an insignificant influence on the simulation results. Therefore, the medium grid with a total number of 2.29 million grids (i.e., Mesh3) is used for the following simulations.

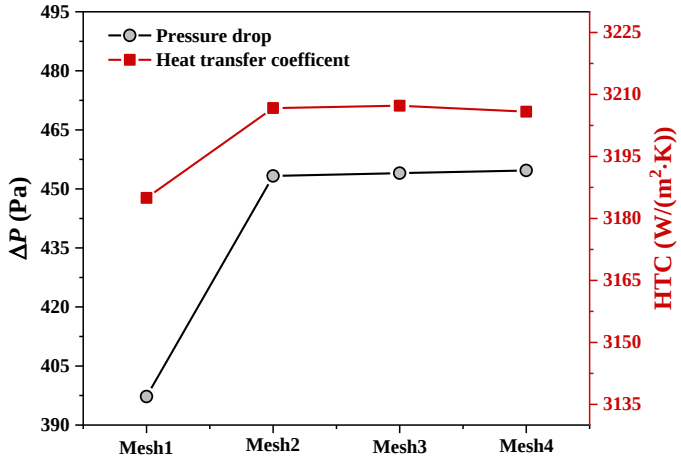

Fig. S6 Pressure drop (ΔP) and heat transfer coefficient (HTC) under different grid resolutions

S2.3 Model validation

The operating conditions and boundary conditions of the simulations for the validation refer to the design conditions. The model is validated by comparing the predicted results with the design values, as shown in Table S4. The pressure drop of the condenser is slightly higher than the design value, with a relative error of 13.5%, which is acceptable for such an industrial-scale apparatus. The condensation ratio from the simulation results is consistent with that from the design value, with a relative error of 0.3%. Moreover, the predicted heat transfer coefficient is comparable to the design value, with a relative error of 2.0%. The results confirm the reasonability of the established model in predicting fluid dynamics and condensation behaviours.

Table S4 Comparison of simulation results with design parameters

Performance indicator	Design value	Simulation result	Error
Pressure drops (Pa)	400	454.0	13.5%
Condensation ratio (%)	98.5	98.2	0.3%
Heat transfer coefficient (W/(m^2 Ҡ))	3144	3207.28	2.0%

Nomenclature

A	Heat transfer area	m^2
d_{in}, d_{out}	Inner, outer diameter of tubes	m
D_k	Mass diffusion factor	1
g	Gravitational acceleration	m/s^2
h	Heat transfer coefficient	W/(m^2 Ҡ)
L	Latent heat of phase change	kJ/kg
$\dot{m}$	Mass flow rate of condensation	kg/s
m_{air}, m_{vapor}	Mass fraction of air and vapor	-
M_{air}, M_{vapor}	Molecular mass of air and vapor	-
Nu	Nusselt number	-
Pr_{cw}	Prandtl number of cooling-water	-
P_{vapor}	Partial pressure of vapor	Pa
Re_{cw}	Reynolds number of cooling-water	-
R_{cw}, R_w, R_c, R_a	Thermal resistance of cooling-water, tube-wall,	m^2 Ҡ/W

	condensing-film, non-condensable gas	
R_{co}	Thermal resistance of laminar condensation film	m^2 K/W
R_{total}	Total thermal resistance	m^2 K/W
T_w, T_{cs}, T_s	Temperature of tube-wall, condensing-surface, steam	K
Δt_m	Temperature difference	K
λ_{cw}, λ_w, λ_c	Thermal conductivity of cooling-water, tube-wall	W/(m K)
μ_c	Molecular viscosity of condensing-film	kg/(m K)
ρ_c	Density of condensing-film	kg/m^3

References:

Ghiaasiaan SM, 2007. Two-phase flow, boiling, and condensation: in conventional and miniature systems. Cambridge University Press.

Gnielinski V, 1975. New equations for heat and mass transfer in the turbulent flow in pipes and channels. *NASA STI/recon technical report A*, 41 (1): 8-16.

Incropera FP, DeWitt DP, Bergman TL, et al., 1996. Fundamentals of heat and mass transfer, 6. Wiley New York.

Mirzabeygi P, Zhang C, 2015. Three-dimensional numerical model for the two-phase flow and heat transfer in condensers. *International Journal of Heat and Mass Transfer*, 81: 618-637.

Popiel CO, Boguslawski L, 1975. Heat transfer by laminar film condensation on sphere surfaces. *International Journal of Heat and Mass Transfer*, 12 (18): 1486-1488.

Sadek O, Mohany A, Hassan M, 2018. Numerical investigation of the cross flow fluidelastic forces of two-phase flow in tube bundle. *Journal of Fluids and Structures*, 79: 171-186.

Sokolichin A, Eigenberger G, 1999. Applicability of the standard k–ε turbulence model to the dynamic simulation of bubble columns: Part I. Detailed numerical simulations. *Chemical Engineering Science*, 54 (13-14): 2273-2284.